# Preparation, characterization, and efficient chromium (VI) adsorption of phosphoric acid activated carbon from furfural residue: an industrial waste

Hao Zhang, Yiming Sun, Shen Li, Xihui Li, Haifeng Zhou and Yuanyu Tian


## ABSTRACT

Furfural residue (FR) is an inevitable by-product of industrial furfural production. If FR is not managed properly, it will result in environmental problems. In this study, FR was used as a novel precursor for activated carbon (AC) production by $H_3PO_4$ activation under different conditions. Under optimum conditions, the prepared FRAC had high BET surface area (1,316.7 $m^2/g$) and micro-mesoporous structures. The prepared FRAC was then used for the adsorption of Cr(VI). The effect of solution pH, contact time, initial Cr(VI) concentration, and temperature was systematically studied. Characterization of the adsorption process indicated that the experimental data were well-fitted by the Langmuir isotherm model and pseudo-second-order kinetics model. The maximum adsorption capacity of 454.6 mg/g was achieved at pH 2.0, which was highly comparable to the other ACs reported in the literatures. The preparation of FRAC using $H_3PO_4$ activation can make use of FR's characteristic acidity, which could make it preferable in practical industrial production.


**Key words** | activated carbon, Cr(VI) adsorption, furfural residue, phosphoric acid


**Hao Zhang**
**Yiming Sun**
**Xihui Li**
**Haifeng Zhou** (corresponding author)
**Yuanyu Tian**
Key Laboratory of Low Carbon Energy and Chemical Engineering, College of Chemistry and Bioengineering,
Shandong University of Science and Technology,
Qingdao, 277590,
China
E-mail: *zhou_hf@sdust.edu.cn*

**Shen Li**
**Yuanyu Tian**
State Key Laboratory of Heavy Oil Processing,
China University of Petroleum (East China),
Qingdao 266580,
China


## HIGHLIGHTS

- The preparation of FRAC using $H_3PO_4$ activation can make use of FR's characteristic acidity, which could make it preferable in practical industrial production.
- Under optimum conditions, the prepared FRAC had high BET surface area (1316.7 $m^2/g$) and micro-mesoporous structures, the maximum adsorption capacity of Cr at pH 2.0 was 454.6 mg/g, which was highly comparable with other ACs reported in the literature.

## GRAPHICAL ABSTRACT

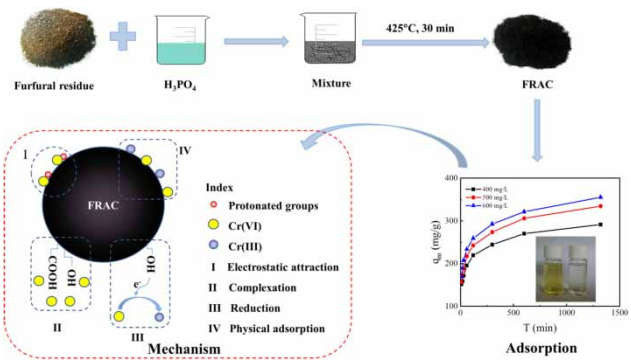


doi: 10.2166/wst.2020.530

## INTRODUCTION

With the development of economic globalization, the problem of water pollution has gradually come into people's sight, among which industrial waste water is the most serious (Khamis *et al.* 2009). Chromium ion pollution is an important aspect of industrial waste water pollution. Some studies have found that chromium ion pollution is serious in many river basins in the world (Islam *et al.* 2015; Scheuhammer *et al.* 2015). The U.S. Environmental Protection Agency (USEPA) has classified chromium (VI) compounds as class A pollutants, which can cause skin problems, gastrointestinal diseases and high carcinogenic risk (Costa & Klein 2008; Desai *et al.* 2008; Wang *et al.* 2020). Therefore, it is meaningful to investigate the removal of chromium ions in waste water. Activated carbon (AC) adsorption is widely used in the removal of heavy metal ions in waste water. The specific surface area of AC is large, and the micropores are particularly developed, which helps to improve the adsorption capacity (Kumar & Mohan Jena 2015). However, commercial AC is usually expensive. In recent years, lots of researches have focused on the preparation of AC to pursue higher adsorption efficiency and lower production price. Agricultural by-products, with the advantages of low cost and renewable nature, have been used as the raw material for the production of AC, such as bamboo leaves, sugarcane bagasse, rice straw, peanut shells, herb residue, reedy grass leaves, jackfruit peel, and pinewood sawdust (Prahas *et al.* 2008; Xu *et al.* 2014; Marzbali *et al.* 2016; Ghosh *et al.* 2017; Yi *et al.* 2019).

Furfural residue (FR) (Zhu *et al.* 2016) is a waste by-product produced from commercial furfural production process. It is reported that approximately 13 tons of furfural residue will be produced per ton of furfural production. The annual emission of FR is huge, having reached 2.4 million to 3 million tons in China. This large amount of FR is a great threat to the environment (Xing *et al.* 2015; Wang *et al.* 2016). Some furfural factories burn FR as a fuel (Ma *et al.* 2014). However, FR contains 14% to 15% acid (Zhu *et al.* 2016), which will corrode the equipment. If this part of acid could be utilized properly, it will be beneficial for enhancing the economics of industrial furfural production.

For preparing AC, physical activation and chemical activation are common methods. Compared with physical activation, chemical activation has the advantages of low activation temperature, short activation time and low energy consumption. Among chemical activation methods, phosphoric acid activation is a hotspot in recent years. Phosphoric acid is a medium-strength acid with dehydrating properties, which enhances the de-polymerization, dehydration, and redistribution of constituent biopolymers (Danish & Ahmad 2018). In the presence of phosphoric acid, pyrolytic decomposition of the macromolecules composing the biomass is improved, including cellulose, lignin, and hemicellulose. In addition, phosphoric acid activation is beneficial for the formation of the cross-linked structure with both micropores and mesopores (Budinova *et al.* 2006; Heidari *et al.* 2014). FR mainly contains cellulose and lignin, which could be used as a precursor for AC production. Using phosphoric acid activation can make full use of the acidity of FR without washing or neutralization, which is conductive to reduce the cost of AC production.

Therefore, in this study, phosphoric acid activation was used to activate fresh FR. The effect of different conditions on AC preparation was explored, such as phosphoric acid dosages, activation temperatures, activation times, and heating rates. The AC prepared under the optimum conditions was characterized by elemental analysis, FT-IR, SEM, $N_2$ physisorption, and XPS. Cr(VI) removal from the waste water was used to evaluate the adsorption performance of AC. The effects of adsorption temperature, solution pH and Cr(VI) concentration on the adsorption efficiency of AC were studied. The adsorption mechanism of Cr(VI) by AC was proposed.

## MATERIALS AND METHODS

### Materials

Fresh furfural residue (FR) was kindly provided by Shandong Kaiyuan Group Co. (Shandong, China). The moisture content of FR was 53%, and the initial pH of FR was around 3.0 (Shi *et al.* 2019). FR was used as received without any treatment. Sym-Diphenylcarbazide was purchased from Shanghai Zhanyun Chemical Co., LTD. HCl, $H_3PO_4$, $H_2SO_4$, $K_2Cr_2O_7$, and acetone came from KeLong Chemical Reagent Factory (Chengdu, China).

### Preparation of activated carbon

10 g of dried FR was suspended in 60 g of $H_3PO_4$ solution (the weight ratio of $H_3PO_4$/FR at 0.5:1 ~ 2:1.) under stirring at

room temperature for 6 h. After impregnation, the mixture was dried at 105 °C. Subsequently, the dried mixture was transferred in a muffle furnace, semi-carbonized at 170 °C for 1 h, and carbonized at different temperature (325 ~ 525 °C) for different holding times (0.5 ~ 3 h), and the heating rate of the muffle furnace was investigated at 3, 8, and 15 °C/min.

After calcination, the material was quenched to increase its hardness. After filtration, the solid was ground and then boiled with 150 mL 0.1 M HCl for half an hour. The final activated carbon (AC) was washed with distilled water, dried at 105 °C for 24 h, and ground into fine powder for further use.

## Characterization

The element contents of FR and AC were determined by an elemental analyzer (Elementar Vario EL III, Flash Smart, Germany). The surface area and pore structure of AC were determined by a Micromeritics ASAP 2460 apparatus at 77 K. The BET surface area ($S_{BET}$) was calculated with Brunauer-Emmett-Teller (BET) method. The total volume ($V_{tot}$) was obtained by single point adsorption of $N_2$ at a high relative pressure (~0.99). The micropores area ($S_{mic}$) and volume ($V_{mic}$) were determined by the t-plot method. The external area ($S_{ext}$) and volume ($V_{ext}$) was calculated from the difference between $S_{BET}$ and $S_{mic}$, $V_{tot}$ and $V_{mic}$, respectively. The pore size distribution was analyzed by DFT method and average pore diameter ($D_P$) was calculated by $4\,V/S_{BET}$. FTIR was investigated by the KBr disk method using Fourier Transform Infrared Spectroscopy (Nicolet iS50 FTIR, Thermo Fisher Scientific) (Liang *et al.* 2020). The FTIR spectrum was taken in a wavelength range of 400–4,000 $cm^{-1}$. The surface characteristics of AC were measured by scanning electron microscopy (SEM) (Apreo, FEI, Hillsboro, USA), operated at the acceleration voltage of 2.0 kV. X-ray photoelectron spectroscopy (XPS) was measured on a VG ESCALAB 250XI spectrometer (Thermo Electron) with an Al K$\alpha$ (1,486 eV) X-ray source.

## Batch adsorption experiments

A certain amount of potassium dichromate was dissolved in distilled water to prepare Cr(VI) solutions of different concentrations. The effect of pH (2–5), adsorption temperature (25–45 °C), contact time (1–120 min) was investigated. The pH value of the solution was adjusted with 0.1 M HCl solution. For each adsorption experiment, 50 mg of AC was added into a 250 mL conical flask containing 40 mL potassium dichromate solution. The mixture was continually stirred in a constant temperature shaker at a fixed shaking rate of 150 rpm. After a given period of time, a certain volume of solution was taken out for centrifugation at 10,000 rpm for 3 min. The supernatant was collected and diluted for Cr(VI) concentration determination at 542 nm by using a UV-visible spectrophotometer.

The removal rate of Cr(VI) by AC can be calculated by $R\% = \frac{C_0 - C_e}{C_0} \times 100\%$. The adsorbed amount of Cr(VI) on AC at equilibrium is calculated by $q_e = \frac{C_0 - C_e}{m} \times V$. The adsorbed amount at $t$ time is calculated by $q_t = \frac{C_0 - C_t}{C_0} \times V$. Where $C_0$ (mg/L) and $C_e$ (mg/L) are the initial concentration and equilibrium concentration of Cr(VI) solution, respectively; $m$ (g) is the mass of AC, V (L) is the volume of Cr(VI) solution.

The flame atomic absorption spectrophotometer (TAS-986F, China) was used to characterize the variation of Cr(VI) and Cr(III) in solution. The concentration of Cr(III) was expressed by the difference between total chromium and Cr(VI).

## Kinetics study

In order to explore the kinetics of Cr(VI) adsorption on AC, the experimental data were fitted by pseudo-first-order (PFO), pseudo-second-order (PSO), and intra-particle diffusion (IPD). They can be expressed by the following equations:

$$\ln(q_e - q_t) = \ln q_e - k_1 t \tag{1}$$

$$\frac{t}{q_t} = \frac{t}{q_e} + \frac{1}{k_2 q_e^2} \tag{2}$$

$$q_t = k_i t^{0.5} + c \tag{3}$$

where $t$ (min) refers to the time during adsorption process, $k_1$ (1/min), $k_2$ (g/(mg min)), and $k_i$ (mg/g $min^{0.5}$) refer to the adsorption rate constant of the PFO equation, PSO equation, and internal diffusion model, respectively.

## Adsorption isotherm

Langmuir, Freundlich and Temkin adsorption isotherm models are used for linear fitting. The linear equation form of the Langmuir, Freundlich and Temkin adsorption

isotherm models is as follows:

$$\frac{C_e}{q_e} = \frac{1}{K_L Q_{\max}} + \frac{C_e}{Q_{\max}} \tag{4}$$

$$\ln q_e = \ln K_F + (\ln C_e)/n \tag{5}$$

$$q_e = \frac{RT}{b_t} \ln K_T + \frac{RT}{b_t} \ln C_e \tag{6}$$

where $K_L$ (L/mg) is the Langmuir constant, $Q_{\max}$ (mg/g) is the maximum adsorption capacity; $K_F$ (L/g) is the Freundlich constant, and 1/n is the dimensionless value which characterizes the heterogeneity of adsorbent surface; R (8.314 J/mol K) is the gas constant and $T$ (K) is the absolute temperature, $K_T$ and $b_t$ is a dimensionless Temkin isotherm constant.

### Thermodynamic study

The thermodynamic parameters, including Gibbs free energy change ($\Delta G^0$), entropy change ($\Delta S^0$), and enthalpy change ($\Delta H^0$), were calculated by the following equations:

$$\ln K_d = -\frac{\Delta H^0}{RT} + \frac{\Delta S^0}{R} \tag{7}$$

$$\Delta G = \Delta H^0 - T\Delta S^0 \tag{8}$$

where $K_d$ (mL/g) is the thermodynamic equilibrium constant, $R$ is the gas constant 8.314 (J/mol/K), $T$ (K) represents the absolute temperature. $\Delta H^0$ and $\Delta S^0$ were calculated from the slope and intercept of the plot of $\ln K_d$ versus *1/T*, respectively (Bedin *et al.* 2016).

## RESULTS AND DISCUSSION

### Effect of AC preparation conditions on Cr(VI) removal

The effect of AC preparation conditions on Cr(VI) removal, including impregnation ratio, carbonization temperature, heating rate, and carbonization time, is shown in Figure 1. With increasing impregnation rate of $H_3PO_4$ and FR, the removal rate of Cr(VI) on prepared AC increased first and then decreased. The appropriate amount of $H_3PO_4$ was beneficial for the formation of pores, promoting the adsorption of Cr(VI) on AC. However, further increased dosage of $H_3PO_4$ might result in the collapse of the AC skeleton, which was not conducive to the adsorption of Cr(VI). In terms of carbonization temperature (Figure 1(b)), the AC prepared at 425 °C possessed the highest removal rate of Cr(VI). Although the removal rate of Cr(VI) by AC prepared at 325 °C was similar to that at 425 °C after 60 min adsorption, the initial 30 min removal rate of Cr(VI) by AC prepared at 425 °C was much higher. Therefore, the carbonization temperature of AC preparation was chosen as 425 °C. According to Figure 1(c), the optimum heating rate was 8 °C/min; the removal rate of Cr(VI) could be achieved at 58.9% without pH adjustment. On the premise of keeping the carbonization temperature of 425 °C and heating rate of 8 °C/min, the effect of carbonization time on Cr(VI) removal by AC was investigated and is shown in Figure 1(d). The holding time played an important role in the adsorption performance of prepared AC. With the extension of holding time, the adsorption performance of AC significantly decreased. According to the adsorption capacity of Cr(VI), the preparation condition of AC from untreated FR was as follows: impregnation rate ($H_3PO_4$ : FR) of 1.5, carbonization temperature of 425 °C, heating rate of 8 °C/min, and carbonization time of 30 min. At this condition, the corresponding AC was prepared and named FRAC.

### Characterization

#### Elemental analysis

A precursor with rich C content is the precondition for the preparation of AC. As shown in Table 1, the C content of FR was up to 49.79%, which was an excellent precursor for AC preparation. The S content of FR was 1.62%, which was attributed to the existence of sulfuric acid in FR material because the FR used for FRAC preparation was without any treatment. In terms of FRAC, the C content increased to 60.46%. The O content decreased from 42.25% to 33.81%. FRAC was rich in oxygen-containing groups, which was beneficial for the adsorption of Cr(VI). In addition, there was 1.15% of N in FRAC, which might originate from the N in the raw material corncob.

#### $N_2$ physisorption

Figure 2(a) showed the $N_2$ adsorption-desorption curve of FRAC, which could be classified as an intermediate between Type I and IV according to the IUPAC. When $P/P_0$ was in the range of 0–0.2, the adsorbed volume increased rapidly with increasing $P/P_0$, which might be attributed to the filling of micropores (Zhang *et al.* 2004). It indicated that the prepared FRAC contained microporous structures. The

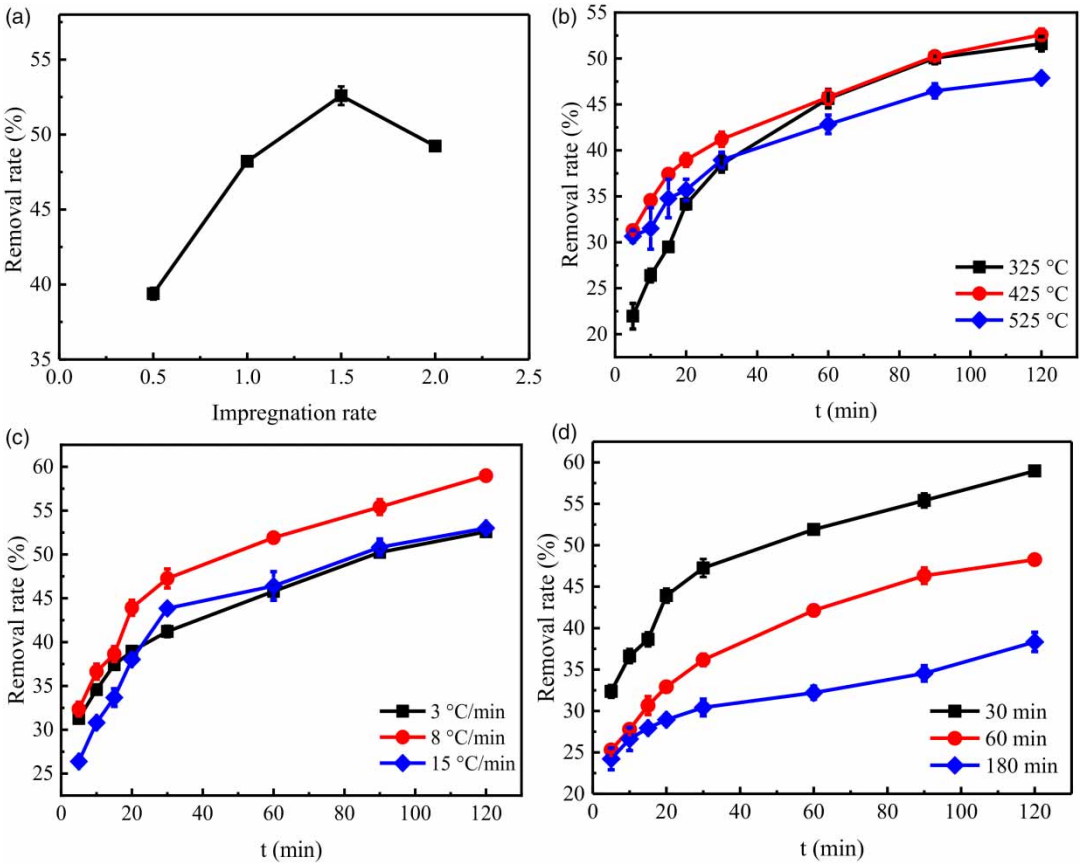


**Figure 1** | Effect of AC preparation conditions on Cr(VI) removal rate: (a) impregnation ratio; (b) carbonization temperature; (c) heating rate; (d) carbonization time (adsorption experiment: initial Cr(VI) concentration; 50 mg/L; temperature, 35 °C; adsorption time, 120 min).

**Table 1** | Elemental analysis of FR and AC

| | Elemental content (wt.%) | | | | |
|---|---|---|---|---|---|
| **Material** | **H** | **C** | **N** | **S** | **O** |
| FR | 5.72 | 49.79 | 0.62 | 1.62 | 42.25 |
| FRAC | 4.48 | 60.46 | 1.15 | ~0.1 | 33.81 |

hysteresis loop of type H4 at high $P/P_0$ ($\geq$0.45) was observed, which was related to the capillary condensation in mesoporous structures (Brito *et al.* 2018). As observed in Figure 2(b), the pore size distribution of the prepared FRAC demonstrated the combination of microporous and mesoporous structures. The pore size distribution was wide with a range of pore widths from 0.4 to 50 nm. Table 2 lists the

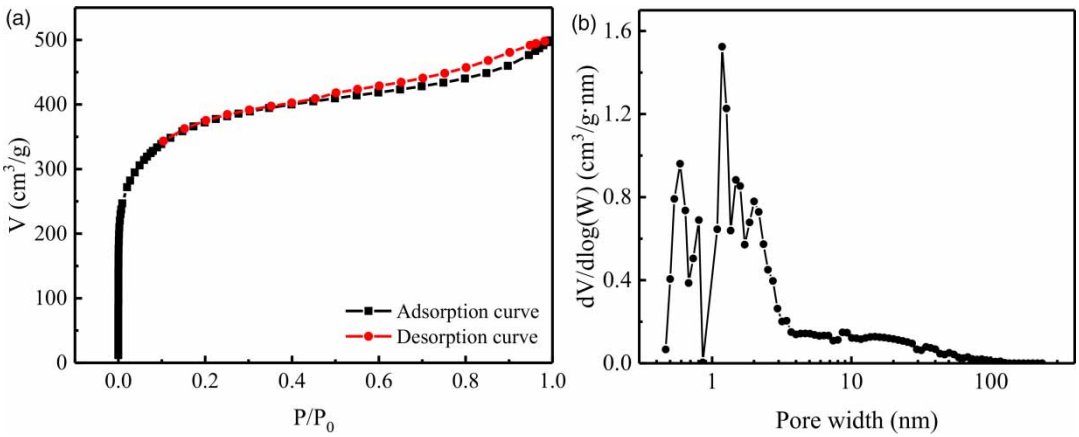


**Figure 2** | $N_2$ adsorption-desorption isotherms (a) and pore size distribution curve (b) of the obtained FRAC.

**Table 2** | Porous structure parameters of FRAC

| Sample | $S_{BET}$ ($m_2$/g) | $S_{mic}$ ($m_2$/g) | $S_{ext}$ ($m_2$/g) | $V_{tot}$ ($cm^3$/g) | $V_{mic}$ ($cm^3$/g) | $V_{ext}$ ($cm^3$/g) | $D_P$ (nm) |
|---|---|---|---|---|---|---|---|
| FRAC | 1,316.7 | 648.8 | 668.0 | 0.769 | 0.280 | 0.489 | 2.335 |

porous structural parameters of FRAC. The $S_{BET}$ of FRAC was as high as 1,316.7 $m^2$/g with 49.3% (648.8 $m^2$/g) of micropores. The $V_T$ of FRAC was 0.769 $cm^3$/g with 36.4% (0.280 $cm^3$/g) of micropores. The $D_P$ of FRAC was 2.355 nm. Micropores could provide lots of adsorption sites, while mesopores are beneficial for the transfer of heavy metal ions (Ma *et al.* 2019). The $S_{BET}$ of FRAC was much superior to that from raw material FR with other activation methods, such as hydrothermal microwave activation (Khushk *et al.* 2020), self-activation (Wang *et al.* 2001), water vapor activation (Yin *et al.* 2014), or pyrolysis auto-activation (Yin *et al.* 2018). In addition, BET surface area comparison of FRAC with other biomass AC using $H_3PO_4$ as the activator is listed in Table 3.

## FTIR

Figure 3 shows the FTIR spectrum of FRAC. The broad peak at 3,800–3,000 $cm^{-1}$ originated from the stretching vibration of –OH from carboxyls, phenols or alcohols, as well as adsorbed water in FRAC (Xu *et al.* 2014). The peaks at 2,927 and 2,847 $cm^{-1}$ were assigned to C-H stretching in the methyl and methylene groups (Zhou *et al.* 2020). The sharp peak at 1,610 and 1,395 $cm^{-1}$ was attributed to the stretching vibration of C = O and C-O in the carboxyl groups, respectively (Maneerung *et al.* 2016). The band in the range of 1,300–1,000 $cm^{-1}$ is usually attributed to C-O stretching (Benadjemia *et al.* 2011). However, the characteristic of phosphorus and phosphocarbonaceous compounds in $H_3PO_4$ activated carbons is also in this range. The peak

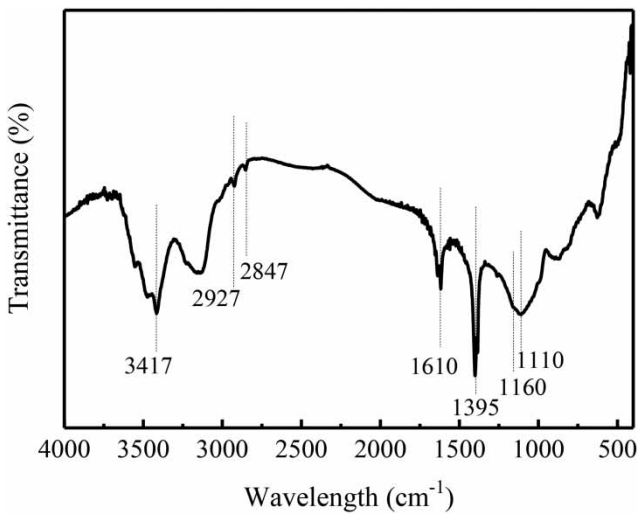


**Figure 3** | FTIR spectrum of FRAC.

around 1,160 $cm^{-1}$ originated from the stretching mode of hydrogen-bonded $P=OOH$ groups from phosphates or polyphosphates, and the O-C stretching vibration in the P-O-C (aromatic) linkage (Xu *et al.* 2014). The peak at 1,110 $cm^{-1}$ might be attributed to $P^{+}$-$O^{-}$ in acid phosphate esters as well as the symmetrical vibration in polyphosphate chain P-O-P (Puziy *et al.* 2007). Therefore, the prepared FRAC contained a large number of surface functional groups, such as hydroxyl groups, carboxylic groups.

**Table 3** | BET surface area of AC from different biomasses with $H_3PO_4$ as the activator

| Biomass | $S_{BET}$ ($m^2$/g) | Reference |
|---|---|---|
| Water hyacinth | 423.6 | Huang *et al.* (2014) |
| Yellowmombin fruit stones | 511.0 | Brito *et al.* (2018) |
| *Arundo donax* Linn | 675.0 | Sun *et al.* (2016) |
| Lotus stalks | 1,179.0 | Liu *et al.* (2013) |
| Pomelo peel | 1,252.0 | Sun *et al.* (2016) |
| Jackfruit peel | 1,260.0 | Prahas *et al.* (2008) |
| Birch | 1,360.0 | Budinova *et al.* (2006) |
| Reedy grass leaves | 1,474.0 | Xu *et al.* (2014) |
| FR | 1,316.7 | This study |

## SEM

The morphology of FRAC was investigated by SEM. The surface microstructures of FRAC were observed under 100,000 times magnification. As shown in Figure 4(a), a highly porous structure with various sizes and shapes was observed, which was consistent with the BET results of FRAC. The pores on the surface of FRAC were mainly caused by the evaporation of activator $H_3PO_4$ (Demiral *et al.* 2008). The porous structure of FRAC was beneficial for the adsorption of Cr(VI) on FRAC. After Cr adsorption, the surface became rough and some of the pores collapsed. In addition, the EDS and Cr mapping showed that a large number of Cr ions were detected on FRAC.

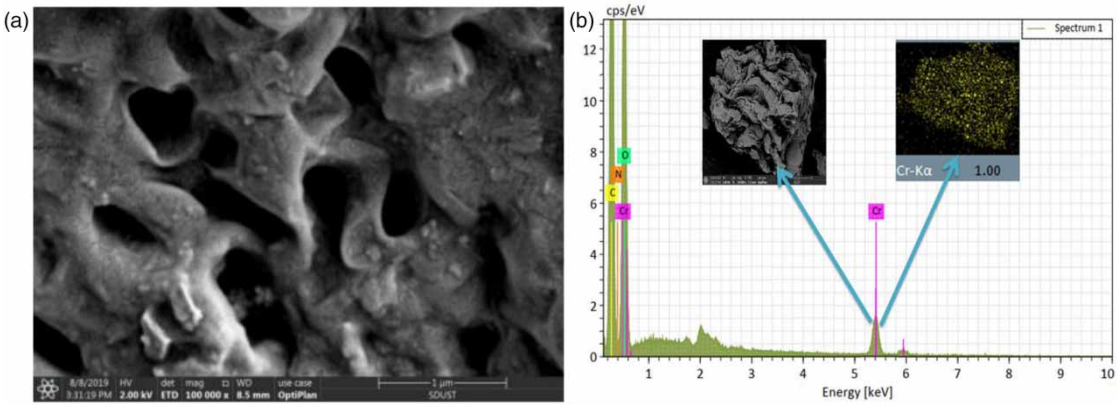


**Figure 4** | SEM of FRAC before Cr(VI) adsorption (a) and SEM, EDS, and Cr mapping of Cr-loaded FRAC (b).

## XPS

XPS analysis was used to investigate the chemical composition changes of FRAC before and after Cr(VI) (FRAC-Cr) adsorption. As observed in Figure 5(a), compared to FRAC, two new peaks assigned to Cr 2p at 587.1 and 577.3 eV are clearly observed in the spectrum of FRAC-Cr, indicating that Cr was on the surface of FRAC. In order to obtain more information about the adsorption process, the high resolution spectra of C 1s, O 1s, and Cr 2p were further analyzed. As shown in Figure 5(b), the characteristic bands of C 1 s presented at 284.7, 285.3, and 287.6 eV, assigned to graphitized carbon, carbon species in alcohol, phenols, ether groups, and/or C-O-P linkage, and carbon in carbonyl groups (Xu *et al.* 2014). After adsorption of Cr, the peak contribution at 287.6 eV increased, while the peak contribution at 285.3 eV decreased. This might be due to the oxidation of hydroxyl groups into carbonyl groups. Figure 5(c) exhibits the high resolution spectra of O 1s. The O 1s spectra could be fitted into three peaks, at 531.4, 532.6, and 533.4 eV, which are characteristic of oxygen double bond in carboxylic groups (C = O) and non-bridging oxygen in the phosphate group ($P = O$), singly bonded oxygen in C-O and C-O-P groups, and –O-H, respectively (Puziy *et al.* 2008; Liu *et al.* 2018). After the adsorption of Cr(VI), the same three peaks still existed; however, the intensity of C-O and –O-H decreased. On the contrary, the intensity of the oxygen double bond increased, which might be

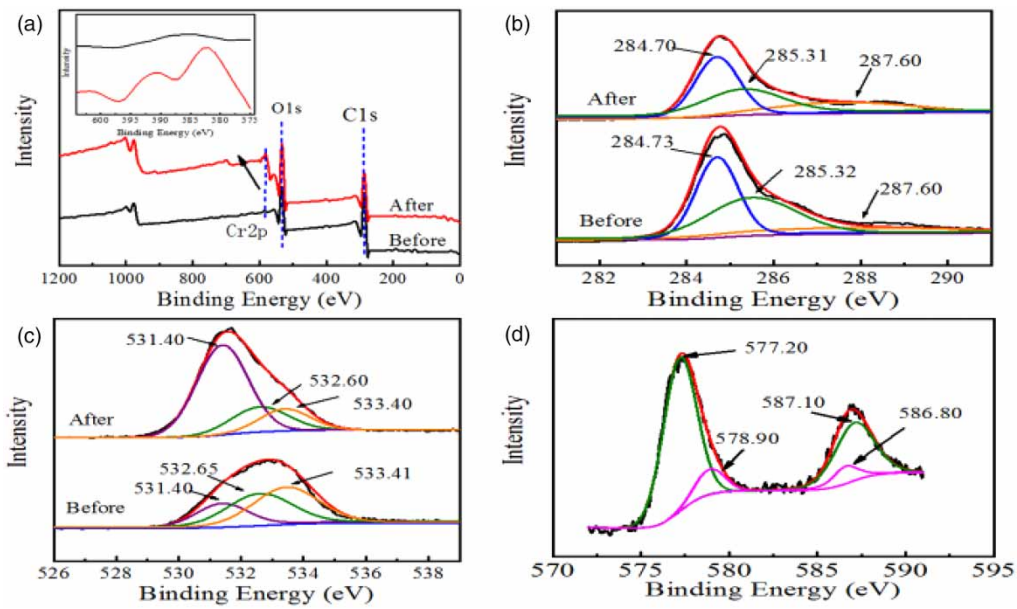


**Figure 5** | XPS survey spectra of FRAC before and after Cr adsorption (a), high resolution XPS spectra of C 1 s (b), O 1 s (c), and Cr 2p after Cr adsorption (d).

attributed to chemisorption during Cr(VI) adsorption on FRAC. As shown in Figure 5(d), the Cr 2p peaks could be fitted into two peaks. The binding energy peaks at 577.2 and 586.8 eV were indexed as Cr(III), which indicated that the Cr(VI) was reduced and adsorbed on FRAC in the form of Cr(III). The binding energy peaks at 578.9 and 587.1 eV corresponded to Cr(VI), indicating the existence of Cr(VI).

## Adsorption performance

### Effect of solution pH

As observed in Figure 6, the removal rate of Cr(VI) was greatly affected by the solution pH. With increasing pH in the range of 2–5, the removal rate of Cr(VI) by FRAC significantly decreased. The maximum removal rate was 99% at pH = 2. The adsorption of Cr(VI) was not only related to the surface functional groups, but also the chemistry of the Cr(VI) solution, which both varied with the solution pH. According to the solution pH, there might be different forms of hexavalent chromium ions, such as $HCrO_4^-$, $Cr_2O_7^{2-}$, $CrO_4^{2-}$. In the pH range of 2–5, the main forms of Cr(VI) were $HCrO_4^-$ and $Cr_2O_7^{2-}$. At pH 2, $HCrO_4^-$ is the dominant form of Cr(VI) (Shi *et al.* 2020). With increasing pH, the dominant form of chromium ions changed to $Cr_2O_7^{2-}$. Due to the smaller ionic size, $HCrO_4^-$ was more conducive to adsorption on FRAC than $Cr_2O_7^{2-}$ (Liu *et al.* 2010). In addition, the highly protonated and positively charged surface at lower pH was beneficial for the adsorption of Cr(VI) anions by electrostatic attraction. With increasing pH, the protonation extent of surface groups decreased; meanwhile, there was competition between $OH^-$ and Cr(VI) anions. Therefore, the removal rate significantly decreased.

FRAC was prepared from raw FR (pH around 3.0) without any treatment and $H_3PO_4$ was used as the activator. Therefore, the unwashed FRAC contained a large number of acids, which might be directly utilized for adjusting the initial pH of the Cr(VI) solution. The pH value of the prepared Cr(VI) solution was close to 5.2. After the addition of 50 mg unwashed FRAC, the pH value of the mixture was close to 2.7. As observed in Figure 6, the removal rate of Cr(VI) by unwashed FRAC was between pH 2.0 and pH 3.0. This indicated that unwashed FRAC could be used for Cr(VI) adsorption directly. It is a promising absorbent candidate for Cr(VI) uptake in industry since the washing procedure of AC and adjustment of Cr(VI) waste water pH can be omitted.

### Adsorption kinetics

The effect of contact time on Cr(VI) adsorption at different initial Cr(VI) concentrations of 400, 500, and 600 mg/L is shown in Figure 7. Due to a large number of available adsorption sites in the beginning, a rapid increase was observed during the first 120 min. Subsequently, the adsorption rate became slow and finally achieved equilibrium. At initial Cr(VI) concentrations of 400, 500, and 600 mg/L, the adsorption capacity was 291.5, 334.6, and 355.3 mg/g, respectively. The increase of adsorption capacity might be due to the larger concentration gradient between Cr(VI) in

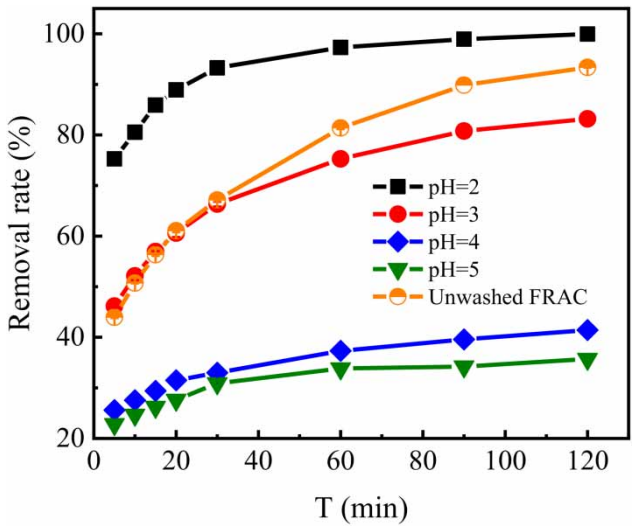


**Figure 6** | Effect of pH on adsorption properties of FRAC.

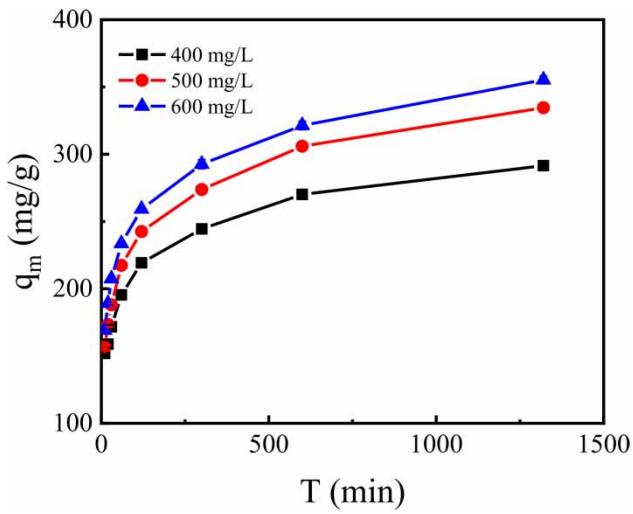


**Figure 7** | Effect of contact time on adsorption of Cr(VI) at different initial concentrations.

solution and FRAC. Nevertheless, the removal rate of Cr(VI) decreased from 91.1% to 74.0% with Cr(VI) concentration increase from 400 to 600 mg/L.

In order to further explore the kinetics and the possible mechanism of Cr(VI) adsorption on FRAC, three commonly used kinetic models (PFO, PSO, and IPD) were employed to simulate the process. The plots of different kinetic models fitting for the adsorption of Cr(VI) on FRAC is shown in Figure S1 (Supplementary Information). The fitting parameters of different kinetic models are shown in Table 4. The regression coefficient $R^2$ and the difference between $q_e$ and $q_{e\ (exp)}$ were utilized to estimate the correlation of these models. Compared with the PSO model, the PFO model exhibited lower values of $R^2$. Moreover, the consistency between $q_e$ and $q_{e\ (exp)}$ was worse; for instance, the $q_{e\ (exp)}$ was 291.5, 334.6, and 355.3 mg/g for initial Cr(VI) concentrations of 400, 500, and 600 mg/L, respectively, while it was only 142.6, 163.5, and 170.2 mg/g for PFO calculated $q_e$. In terms of PSO, excellent consistency existed between $q_e$ and $q_{e\ (exp)}$, indicating that a chemical adsorption might be the rate-limiting step, which involved valence forces through sharing of electrons between Cr(VI) and FRAC (Mohan *et al.* 2011).

In order to explore the diffusion mechanism, the IPD model was used to fit the experimental data. The adsorption process is a multi-step process, usually containing outer diffusion (also called film diffusion), inner diffusion (also called intra-particle diffusion), and adsorption of adsorbate onto the active sites on the outer and/or inner surface of the adsorbent through strong adsorbate-adsorbent interactions equivalent to covalent bond formation or weak adsorption very similar to van der Waals forces (Singh *et al.* 2012). However, the last step is very quick, and is usually not the rate-limiting step. Therefore, the adsorption process is usually controlled by either the outer diffusion or inner diffusion or both. As shown in Figure S1(c), the plot of $q_t$ versus $t^{0.5}$ exhibited multi-linearity; moreover, it did not pass through the origin. Therefore, the intra-particle diffusion was not the only rate-limiting step.

**Table 4** | Fitting parameters of different kinetic models

| | | Initial Cr(VI) concentrations | | |
|---|---|---|---|---|
| **Dynamic model** | **Parameters** | **400 mg/L** | **500 mg/L** | **600 mg/L** |
| – | $q_{e\ (exp)}$ (mg/g) | 291.5 | 334.6 | 355.3 |
| PFO | $k_1$ (1/min) | 0.00396 | 0.00308 | 0.00306 |
| | $q_e$ (mg/g) | 142.9 | 163.5 | 170.2 |
| | $R^2$ | 0.9836 | 0.9921 | 0.9876 |
| PSO | $k_2$ (g/mg/min) | 0.00340 | 0.00296 | 0.00279 |
| | $q_e$ (mg/g) | 294.1 | 337.8 | 358.4 |
| | $R^2$ | 0.9982 | 0.9976 | 0.9973 |
| IPD | $k_{id1}$ (mg/g $min^{0.5}$) | 9.805 | 13.325 | 14.031 |
| | $c_1$ | 118.34 | 114.39 | 126.49 |
| | $k_{id2}$ (mg/g $min^{0.5}$) | 4.960 | 5.742 | 6.035 |
| | $c_2$ | 160.16 | 175.63 | 189.38 |
| | $k_{id3}$ (mg/g $min^{0.5}$) | 2.407 | 3.122 | 3.252 |
| | $c_3$ | 205.99 | 223.44 | 238.39 |
| | $R^2$ | 0.9722 | 0.9845 | 0.9897 |

## Adsorption isotherms

The adsorption isotherms study was studied at three different temperatures (25, 35, and 45 °C) with the initial Cr(VI) concentration of 350–1,000 mg/L at pH 2.0. Three isotherm models were used to simulate the experimental data. The model parameters of Langmuir, Freundlich, and Temkin (plot figures shown in Figure S2) are listed in Table 5. The higher $R^2$ value of the Langmuir model indicated that the adsorption of Cr(VI) on FRAC was better fitted by this model. This suggested that the adsorption occurred on a homogeneous adsorbent surface (Sun *et al.* 2016; Duan *et al.* 2017). The maximum monolayer capacity ($q_m$) increased from 400.0 to 454.6 mg/g. The adsorption capacity of Cr(VI) exhibited an upward trend with increasing temperature. It indicated that the adsorption process of Cr(VI) on FRAC was endothermic and higher temperature was conducive to improve the process. For evaluating the adsorption capacity of Cr(VI) on FRAC, the comparison of $q_m$ calculated from Langmuir with other AC prepared using different raw materials or different methods is listed in Table 6. From the comparison, it can be seen that the FRAC produced in this study exhibited higher $q_m$, indicating an excellent adsorption efficiency for Cr(VI).

**Table 5** | Isothermal parameters for Cr(VI) adsorption by FRAC at different temperatures

| | | Temperature (°C) | | |
|---|---|---|---|---|
| **Isotherms** | **Parameters** | **25** | **35** | **45** |
| Langmuir | $K_L$ (L/g) | 0.051 | 0.059 | 0.096 |
| | $q_m$ (mg/g) | 400.0 | 434.8 | 454.6 |
| | $R^2$ | 0.9972 | 0.9982 | 0.9916 |
| Freundlich | $K_F$ (mg/g $(L/mg)^{1/n}$) | 152.19 | 198.50 | 216.09 |
| | 1/n | 0.1608 | 0.1209 | 0.1271 |
| | $R^2$ | 0.8969 | 0.8960 | 0.7721 |
| Temkin | $K_T$ (L/mg) | 4.675 | 51.227 | 49.418 |
| | $b_t$ | 47.163 | 62.364 | 56.975 |
| | $R^2$ | 0.9062 | 0.8843 | 0.7079 |

**Table 6** | Comparisons of adsorption capacity for Cr(VI) by various adsorbents

| Adsorbents | pH | $q_m$ (mg/g) | Reference |
|---|---|---|---|
| AC produced from FR | 4 | 7.6 | Chen *et al.* (2010) |
| Longan seed AC | 3 | 35.0 | Yang *et al.* (2015) |
| AC produced from FR | 2 | 36.9 | Khushk *et al.* (2020) |
| Bael fruit shell AC | 2 | 43.5 | Gottipati & Mishra (2016) |
| Magnetic AC from termite feces | 4 | 66.0 | Demarchi *et al.* (2019) |
| AC produced from lignin | 2 | 77.9 | Albadarin *et al.* (2011) |
| corn straw biochar | 3 | 175.4 | Ma *et al.* (2019) |
| AC produced from date press cake | 2 | 282.8 | Norouzi *et al.* (2018) |
| Amino-functionalized hydrochars | 2 | 363.2 | Ghadikolaei *et al.* (2019) |
| FRAC | 2 | 454.6 | This study |

## Adsorption thermodynamics

The linear fitting of lnKd and 1/T is shown in Figure S3, and the calculated thermodynamic parameters are tabulated in Table 7. The value of $\Delta G^0$ was negative, indicating the spontaneous nature of Cr(VI) adsorption on FRAC. Moreover, at higher temperature, the $\Delta G^0$ value was more negative, indicating that the adsorption process was more favorable at higher temperature. The value of $\Delta H^0$ was positive, further proving the endothermic nature of the adsorption process. In addition, the value of $\Delta S^0$ was positive, suggested that there was an increase in the randomness at the solid-liquid interface during the adsorption process (Demiral *et al.* 2008). Similar findings have been reported for Cr(VI) adsorption by other groups (Demiral *et al.* 2008; Ma *et al.* 2019).

**Table 7** | Calculated thermodynamic parameters for Cr(VI) adsorption on FRAC

| T (°C) | $\ln K_d$ | $\Delta G^0$ (KJ/mol) | $\Delta H^0$ (KJ/mol) | $\Delta S^0$ (KJ/mol/°C) |
|---|---|---|---|---|
| 25 | 1.76 | −4.37 | 15.91 | 0.07 |
| 35 | 2.00 | −5.11 | | |
| 45 | 2.17 | −5.73 | | |

## Cr species in solution

According to the XPS results, there were Cr(III) ions immobilized on the surface of FRAC. In order to explore whether all Cr(III) was adsorbed by FRAC, the variation tendency of total Cr, Cr(VI) and Cr(III) in solution at initial Cr(VI) concentrations of 600 and1,000 mg/L was investigated. As shown in Figure 8, with increasing contact time, the total Cr concentration gradually declined, therefore the removal efficiency of Cr(VI) increased. The Cr(III) was detected in the solution, especially in the initial stage of adsorption. However, with the extension of adsorption time, the content of Cr(III) significantly decreased. After 48 h adsorption, the content of Cr(III) in solution was close to 0. This indicated that a proportion of Cr(VI) was reduced to Cr(III). Moreover, FRAC was also capable of adsorbing Cr(III).

## Adsorption mechanism

The adsorption mechanism of Cr(VI) by FRAC is illustrated in Figure 9. The mechanism could be concluded to the following four parts: (1) The electrostatic attraction between the positively charged FRAC and negatively charged Cr(VI), mainly $HCrO_4^-$ at pH 2.0, was beneficial for the adsorption of Cr(VI) by FRAC; (2) complexation between

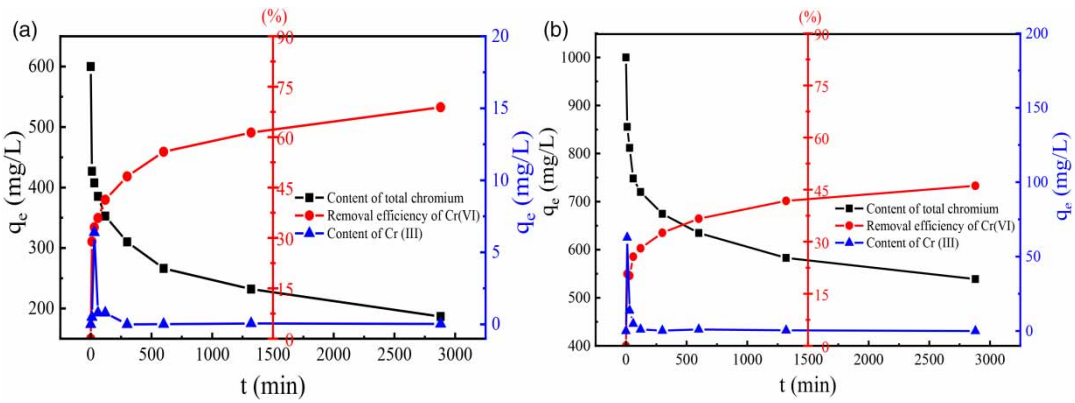


**Figure 8** | The variation tendency of total Cr, Cr(VI) and Cr(III) in solution at different initial Cr(VI) concentrations (a: 600 mg/L; b: 1,000 mg/L).

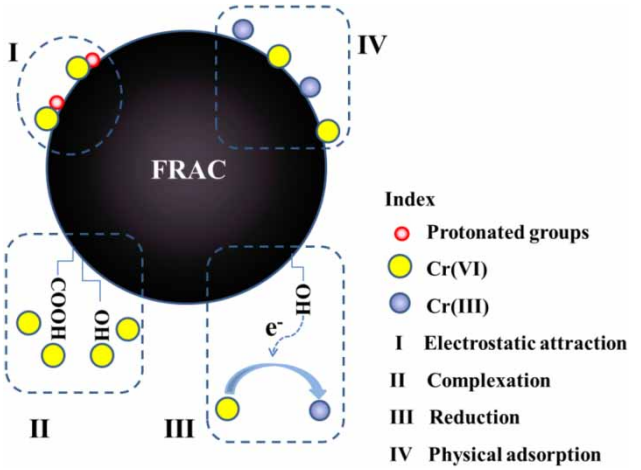


**Figure 9** | Adsorption mechanism of Cr(VI) by FRAC.

Cr(VI) and oxygen-containing functional groups (Equations (9) and (10)); (3) reduction of Cr(VI) to Cr(III) by the adjacent electron donor groups (Equations (11)), such as hydroxyl groups; and (4) physical adsorption of Cr(VI) and Cr(III) by porous FRAC.

$$-\mathrm{COOH} + \mathrm{HCrO_4^-} \rightarrow -\mathrm{COOH}\cdots\mathrm{HCrO_4^-} \quad (9)$$

$$-\mathrm{OH} + \mathrm{HCrO_4^-} \rightarrow -\mathrm{OH}\cdots\mathrm{HCrO_4^-} \quad (10)$$

$$\mathrm{HCrO_4^-} + 3\mathrm{e^-} + 7\mathrm{H^+} \rightarrow \mathrm{Cr^{3+}} + 4\mathrm{H_2O} \quad (11)$$

## CONCLUSION

The $H_3PO_4$-activated porous carbon with high surface area (1,316.7 $m^2/g$) and excellent Cr(VI) adsorption capacity has been successfully prepared from the furfural residue waste. The kinetics and isotherm studies illustrated that the adsorption of Cr(VI) by FRAC was better described by the PSO and Langmuir models. According to the Langmuir model, the maximum adsorption capacity of Cr(VI) on FRAC was 454.6 mg/g. The adsorption mechanism could be summarized as electrostatic attraction, complexation, reduction, and physical adsorption. Therefore, furfural residue could be considered as a promising precursor for the production of AC. Moreover, $H_3PO_4$ activation could utilize the acidity of furfural residue itself. FRAC has a considerable potential for Cr(VI) removal from aqueous solution.

## ACKNOWLEDGEMENTS

The authors would like to acknowledge the financial support of Qingchuang Science and Technology Program of Shandong Province University (2019KJD004), and SDUST Research Fund (2018YQJH102, S202010424057).

## DATA AVAILABILITY STATEMENT

All relevant data are included in the paper or its Supplementary Information.

## REFERENCES

Albadarin, A. B., Al-Muhtaseb, A. a. H., Walker, G. M., Allen, S. J. & Ahmad, M. N. M. 2011 Retention of toxic chromium from aqueous phase by $H_3PO_4$-activated lignin: effect of salts and desorption studies. *Desalination* **274** (1–3), 64–73.

Bedin, K. C., Martins, A. C., Cazetta, A. L., Pezoti, O. & Almeida, V. C. 2016 KOH-activated carbon prepared from sucrose spherical carbon: adsorption equilibrium, kinetic and thermodynamic studies for Methylene Blue removal. *Chemical Engineering Journal* **286**, 476–484.

Benadjemia, M., Millière, L., Reinert, L., Benderdouche, N. & Duclaux, L. 2011 Preparation, characterization and Methylene Blue adsorption of phosphoric acid activated carbons from globe artichoke leaves. *Fuel Processing Technology* **92** (6), 1203–1212.

Brito, M. J. P., Veloso, C. M., Santos, L. S., Bonomo, R. C. F. & Fontan, R. d. C. I. 2018 Adsorption of the textile dye Dianix® Royal Blue CC onto carbons obtained from yellow mombin fruit stones and activated with KOH and $H_3PO_4$: kinetics, adsorption equilibrium and thermodynamic studies. *Powder Technology* **339**, 334–343.

Budinova, T., Ekinci, E., Yardim, F., Grimm, A., Björnbom, E., Minkova, V. & Goranova, M. 2006 Characterization and application of activated carbon produced by $H_3PO_4$ and water vapor activation. *Fuel Processing Technology* **87** (10), 899–905.

Chen, C. J., Wei, L. B., Zhao, P. C., Li, Y., Hu, H. Y. & Qin, Y. B. 2010 Study on preparation of activated carbon from corncob furfural residue with $ZnCl_2$ by microwave irradiation. *Advanced Materials Research* **152–153**, 1322–1327.

Costa, M. & Klein, C. B. 2008 Toxicity and carcinogenicity of chromium compounds in humans. *Critical Reviews in Toxicology* **36** (2), 155–163.

Danish, M. & Ahmad, T. 2018 A review on utilization of wood biomass as a sustainable precursor for activated carbon production and application. *Renewable and Sustainable Energy Reviews* **87**, 1–21.

Demarchi, C. A., Michel, B. S., Nedelko, N., Ślawska-Waniewska, A., Dłużewski, P., Kaleta, A., Minikayev, R., Strachowski, T., Lipińska, L., Dal Magro, J. & Rodrigues, C. A. 2019

Preparation, characterization, and application of magnetic activated carbon from termite feces for the adsorption of Cr(VI) from aqueous solutions. *Powder Technology* **354**, 432–441.

Demiral, H., Demiral, İ., Tümsek, F. & Karabacakoğlu, B. 2008 Adsorption of chromium(VI) from aqueous solution by activated carbon derived from olive bagasse and applicability of different adsorption models. *Chemical Engineering Journal* **144** (2), 188–196.

Desai, C., Jain, K. & Madamwar, D. 2008 Evaluation of in vitro Cr(VI) reduction potential in cytosolic extracts of three indigenous Bacillus sp. isolated from Cr(VI) polluted industrial landfill. *Bioresource Technology* **99** (14), 6059–6069.

Duan, X., Srinivasakannan, C., Wang, X., Wang, F. & Liu, X. 2017 Synthesis of activated carbon fibers from cotton by microwave induced $H_3PO_4$ activation. *Journal of the Taiwan Institute of Chemical Engineers* **70**, 374–381.

Ghadikolaei, N. F., Kowsari, E., Balou, S., Moradi, A. & Taromi, F. A. 2019 Preparation of porous biomass-derived hydrothermal carbon modified with terminal amino hyperbranched polymer for prominent Cr(VI) removal from water. *Bioresource Technology* **288**, 121545.

Ghosh, S. K., Hajra, A. K. & Bandyopadhyay, A. 2017 Air agitated tapered bubble column adsorber for hazardous dye (crystal violet) removal onto activated ($ZnCl_2$) carbon prepared from bamboo leaves. *Journal of Molecular Liquids* **240**, 313–321.

Gottipati, R. & Mishra, S. 2016 Preparation of microporous activated carbon from Aegle Marmelos fruit shell and its application in removal of chromium(VI) from aqueous phase. *Journal of Industrial and Engineering Chemistry* **36**, 355–363.

Heidari, A., Younesi, H., Rashidi, A. & Ghoreyshi, A. 2014 Adsorptive removal of $CO_2$ on highly microporous activated carbons prepared from *Eucalyptus camaldulensis* wood: effect of chemical activation. *Journal of the Taiwan Institute of Chemical Engineers* **45** (2), 579–588.

Huang, Y., Li, S., Chen, J., Zhang, X. & Chen, Y. 2014 Adsorption of Pb(II) on mesoporous activated carbons fabricated from water hyacinth using $H_3PO_4$ activation: adsorption capacity, kinetic and isotherm studies. *Applied Surface Science* **293**, 160–168.

Islam, M. S., Ahmed, M. K., Raknuzzaman, M., Habibullah-Al-Mamun, M. & Islam, M. K. 2015 Heavy metal pollution in surface water and sediment: a preliminary assessment of an urban river in a developing country. *Ecological Indicators* **48**, 282–291.

Khamis, M., Jumean, F. & Abdo, N. 2009 Speciation and removal of chromium from aqueous solution by white, yellow and red UAE sand. *Journal of Hazardous Materials* **169** (1–3), 948–952.

Khushk, S., Zhang, L., Li, A., Irfan, M. & Zhang, X. 2020 Microwave-assisted hydrothermal carbonization of furfural residue for adsorption of Cr(VI): adsorption and kinetic study. *Polish Journal of Environmental Studies* **29** (2), 1671–1681.

Kumar, A. & Mohan Jena, H. 2015 High surface area microporous activated carbons prepared from Fox nut (*Euryale ferox*) shell by zinc chloride activation. *Applied Surface Science* **356**, 753–761.

Liang, Y., Duan, W., An, X., Qiao, Y., Tian, Y. & Zhou, H. 2020 Novel betaine-amino acid based natural deep eutectic solvents for enhancing the enzymatic hydrolysis of corncob. *Bioresource Technology* **310**, 123389.

Liu, W., Zhang, J., Zhang, C., Wang, Y. & Li, Y. 2010 Adsorptive removal of Cr (VI) by Fe-modified activated carbon prepared from *Trapa natans* husk. *Chemical Engineering Journal* **162** (2), 677–684.

Liu, H., Zhang, J., Zhang, C., Bao, N. & Cheng, C. 2013 Activated carbons with well-developed microporosity and high surface acidity prepared from lotus stalks by organophosphorus compounds activations. *Carbon* **60**, 289–291.

Liu, X., He, C., Yu, X., Bai, Y., Ye, L., Wang, B. & Zhang, L. 2018 Net-like porous activated carbon materials from shrimp shell by solution-processed carbonization and $H_3PO_4$ activation for methylene blue adsorption. *Powder Technology* **326**, 181–189.

Ma, B. J., Sun, Y., Lin, K. Y., Li, B. & Liu, W. Y. 2014 Physicochemical pretreatments and hydrolysis of furfural residues via carbon-based sulfonated solid acid. *Bioresource Technology* **156**, 189–194.

Ma, H., Yang, J., Gao, X., Liu, Z., Liu, X. & Xu, Z. 2019 Removal of chromium (VI) from water by porous carbon derived from corn straw: influencing factors, regeneration and mechanism. *Journal of Hazardous Materials* **369**, 550–560.

Maneerung, T., Liew, J., Dai, Y., Kawi, S., Chong, C. & Wang, C.-H. 2016 Activated carbon derived from carbon residue from biomass gasification and its application for dye adsorption: kinetics, isotherms and thermodynamic studies. *Bioresource Technology* **200**, 350–359.

Marzbali, M. H., Esmaieli, M., Abolghasemi, H. & Marzbali, M. H. 2016 Tetracycline adsorption by $H_3PO_4$-activated carbon produced from apricot nut shells: a batch study. *Process Safety and Environmental Protection* **102**, 700–709.

Mohan, D., Sarswat, A., Singh, V. K., Alexandre-Franco, M. & Pittman, C. U. 2011 Development of magnetic activated carbon from almond shells for trinitrophenol removal from water. *Chemical Engineering Journal* **172** (2), 1111–1125.

Norouzi, S., Heidari, M., Alipour, V., Rahmanian, O., Fazlzadeh, M., Mohammadi-moghadam, F., Nourmoradi, H., Goudarzi, B. & Dindarloo, K. 2018 Preparation, characterization and Cr(VI) adsorption evaluation of NaOH-activated carbon produced from Date Press Cake; an agro-industrial waste. *Bioresource Technology* **258**, 48–56.

Prahas, D., Kartika, Y., Indraswati, N. & Ismadji, S. 2008 Activated carbon from jackfruit peel waste by $H_3PO_4$ chemical activation: pore structure and surface chemistry characterization. *Chemical Engineering Journal* **140** (1–3), 32–42.

Puziy, A. M., Poddubnaya, O. I., Martínez-Alonso, A., Castro-Muñiz, A., Suárez-García, F. & Tascón, J. M. D. 2007 Oxygen and phosphorus enriched carbons from lignocellulosic material. *Carbon* **45** (10), 1941–1950.

Puziy, A. M., Poddubnaya, O. I., Socha, R. P., Gurgul, J. & Wisniewski, M. 2008 XPS and NMR studies of phosphoric acid activated carbons. *Carbon* **46** (15), 2113–2123.

Scheuhammer, A., Braune, B., Chan, H. M., Frouin, H., Krey, A., Letcher, R., Loseto, L., Noel, M., Ostertag, S., Ross, P. & Wayland, M. 2015 Recent progress on our understanding of the biological effects of mercury in fish and wildlife in the Canadian Arctic. *Science of The Total Environment* **509–510**, 91–103.

Shi, X., Zhao, B., Zhou, H., Tian, Y., Qiao, Y. & Ji, B. 2019 Direct saccharification and fermentation for high glucose and ethanol production from non-detoxified furfural residue without any pretreatment. *ChemistrySelect* **4** (27), 7844–7850.

Shi, X., Qiao, Y., An, X., Tian, Y. & Zhou, H. 2020 High-capacity adsorption of Cr(VI) by lignin-based composite: characterization, performance and mechanism. *International Journal of Biological Macromolecules* **159**, 839–849.

Singh, S. K., Townsend, T. G., Mazyck, D. & Boyer, T. H. 2012 Equilibrium and intra-particle diffusion of stabilized landfill leachate onto micro- and meso-porous activated carbon. *Water Research* **46** (2), 491–499.

Sun, Y., Li, H., Li, G., Gao, B., Yue, Q. & Li, X. 2016 Characterization and ciprofloxacin adsorption properties of activated carbons prepared from biomass wastes by $H_3PO_4$ activation. *Bioresource Technology* **217**, 239–244.

Wang, Y., Noda, K. & Kagawa, S. 2001 Manufacturing of activated carbon using furfural residue as raw material. *Chemistry Letters* **30** (10), 1052–1053.

Wang, Y., Xu, Z.-y., Song, X., Yang, B. & Zhang, D. 2016 The preparation of low-cost adsorbent for heavy metal based on furfural residue. *Materials and Manufacturing Processes* **32** (1), 87–92.

Wang, X., Xu, J., Liu, J., Liu, J., Xia, F., Wang, C., Dahlgren, R. A. & Liu, W. 2020 Mechanism of Cr(VI) removal by magnetic greigite/biochar composites. *Science of The Total Environment* **700**, 134414.

Xing, Y., Bu, L., Sun, D., Liu, Z., Liu, S. & Jiang, J. 2015 High glucose recovery from direct enzymatic hydrolysis of bisulfite-pretreatment on non-detoxified furfural residues. *Bioresource Technology* **193**, 401–407.

Xu, J., Chen, L., Qu, H., Jiao, Y., Xie, J. & Xing, G. 2014 Preparation and characterization of activated carbon from reedy grass leaves by chemical activation with $H_3PO_4$. *Applied Surface Science* **320**, 674.

Yang, J., Yu, M. & Chen, W. 2015 Adsorption of hexavalent chromium from aqueous solution by activated carbon prepared from longan seed: kinetics, equilibrium and thermodynamics. *Journal of Industrial and Engineering Chemistry* **21**, 414–422.

Yi, Y., Tu, G., Zhao, D., Tsang, P. E. & Fang, Z. 2019 Biomass waste components significantly influence the removal of Cr(VI) using magnetic biochar derived from four types of feedstocks and steel pickling waste liquor. *Chemical Engineering Journal* **360**, 212–220.

Yin, Y. L., Li, A. M. & Zhang, Z. K. 2014 Experimental study on production of activated carbons from furfural residues. *Advanced Materials Research* **878**, 271–277.

Yin, Y., Gao, Y. & Li, A. 2018 Self-activation of biochar from furfural residues by recycled pyrolysis gas. *Waste Management* **77**, 312–321.

Zhang, T., Walawender, W. P., Fan, L. T., Fan, M., Daugaard, D. & Brown, R. C. 2004 Preparation of activated carbon from forest and agricultural residues through $CO_2$ activation. *Chemical Engineering Journal* **105** (1), 53–59.

Zhou, H., Shi, X., Wu, W., An, X., Tian, Y. & Qiao, Y. 2020 Facile preparation of lignosulfonate/N-methylaniline composite and its application in efficient removal of Cr(VI) from aqueous solutions. *International Journal of Biological Macromolecules* **154**, 1194–1204.

Zhu, G.-z., Deng, X.-l., Hou, M., Sun, K., Zhang, Y.-p., Li, P. & Liang, F.-m. 2016 Comparative study on characterization and adsorption properties of activated carbons by phosphoric acid activation from corncob and its acid and alkaline hydrolysis residues. *Fuel Processing Technology* **144**, 255–261.

First received 11 August 2020; accepted in revised form 26 October 2020. Available online 5 November 2020